Development 134, 4083-4093 (2007) doi:10.1242/dev.008524

Selective cortical interneuron and GABA deficits in cyclin D2-null mice

Sara B. Glickstein[1], Holly Moore[2,3], Bozena Slowinska[1], Joelle Racchumi[1], Minah Suh[4], Nao Chuhma[2,3] and M. Elizabeth Ross[1,*]

In contrast to cyclin D1 nulls (*cD1*$^{-/-}$), mice without cyclin D2 (*cD2*$^{-/-}$) lack cerebellar stellate interneurons; the reason for this is unknown. In the present study in cortex, we found a disproportionate loss of parvalbumin (PV) interneurons in *cD2*$^{-/-}$ mice. This selective reduction in PV subtypes was associated with reduced frequency of GABA-mediated inhibitory postsynaptic currents in pyramidal neurons, as measured by voltage-clamp recordings, and increased cortical sharp activity in the EEGs of awake-behaving *cD2*$^{-/-}$ mice. Cell cycle regulation was examined in the medial ganglionic eminence (MGE), the major source of PV interneurons in mouse brain, and differences between *cD2*$^{-/-}$ and *cD1*$^{-/-}$ suggested that cD2 promotes subventricular zone (SVZ) divisions, exerting a stronger inhibitory influence on the p27 Cdk-inhibitor (Cdkn1b) to delay cell cycle exit of progenitors. We propose that cD2 promotes transit-amplifying divisions in the SVZ and that these ensure proper output of at least a subset of PV interneurons.

KEY WORDS: Cyclin D2 (Ccnd2), Parvalbumin interneurons, Cell cycle, Cortical excitability

INTRODUCTION

Comprising 20-30% of cortical neurons, GABAergic interneurons are crucial for the regulation and synchronization of local circuits in cortex and hippocampus (Constantinidis and Goldman-Rakic, 2002). In mice, approximately 80% of cortical interneurons are represented by parvalbumin (PV+), and somatostatin (SSN+) expressing subtypes that are derived from the medial ganglionic eminence (MGE) and follow tangential migrations to the cortex (Xu et al., 2004; Xu et al., 2003). Although, in some settings, they may promote neuron firing (Derchansky et al., 2004), most GABAergic interneurons are inhibitory, raising the depolarization threshold for excitatory neurons. Genetic models indicate that loss of interneuron-mediated GABA transmission can result in lowered seizure threshold. For example, mice without the synthetic enzyme GAD65 (glutamic acid decarboxylase 2; also known as Gad2 – Mouse Genome Informatics) lack the normal postnatal increase in cortical GABA and display paroxysmal electroencephalographic (EEG) spike activity with increased seizure frequency (Stork et al., 2000). Genetic inactivation of uPAR (urokinase plasminogen activator receptor; also known as Plaur – Mouse Genome Informatics) reduces PV-expressing GABAergic interneurons in cingulate and parietal cortex as well as SSN-expressing interneurons in the hippocampus (Eagleson et al., 2005). Mice lacking uPAR have spontaneous seizures and a lowered threshold to pharmacologically induced seizures (Powell et al., 2003). Deletion of the Dlx1 transcription factor reduces calretinin interneurons, becoming apparent by postnatal day 60 (P60), while sparing PV+ subtypes (Cobos et al., 2005). *Dlx1*$^{-/-}$ mice reveal generalized spike and spike-wave EEG patterns in the absence of myoclonic seizures, with higher frequency and amplitude spike discharges during myoclonic seizures. The *uPAR*- and *Dlx*-null mouse mutants suggest that subtype-specific interneuron deficits may be distinguishable, and such selective deficits might yield insight into the function – and perhaps critical developmental emergence – of particular interneuronal subpopulations.

Mice lacking the G1-active cell cycle protein cyclin D2 (cD2; also known as Ccnd2 – Mouse Genome Informatics) display a small cerebellum with loss of granule neurons and virtually no detectable stellate interneurons (Huard et al., 1999). Despite these losses, other interneurons, including basket and Golgi cells as well as Purkinje projection neurons, appear unchanged. *cD2*-null mice also exhibit reduced cerebral cortical volume, suggesting that cell deficits might also be found in the telencephalon. More-recent mapping of cD2 and cyclin D1 (cD1; also known as Ccnd1 – Mouse Genome Informatics) protein expression during brain development indicates that these two cyclins define separate progenitor pools in embryonic brain (Glickstein et al., 2007). However, the forebrain cytoarchitecture has remained unexplored in *cD2*$^{-/-}$ mice.

Here, we have found selective deficits in cortical PV+ interneurons in mice lacking cD2, associated with reduced GABAergic currents and increased cortical irritability. Cell cycle data suggest that cD2 exerts stronger suppression on p27 (also known as p27Kip1 and Cdkn1b – Mouse Genome Informatics) levels than does cD1, to promote progenitor divisions within the subventricular zone (SVZ). These SVZ divisions, which have been termed 'intermediate progenitor' or 'transit amplifying', appear to be crucial for establishing the proper density of PV interneurons, but are not crucial for other subtypes, including SSN neurons, that also derive from the MGE (Wonders and Anderson, 2006).

MATERIALS AND METHODS

Mouse breeding

Cyclin D2 knockouts disrupted exons I and II of the gene (Sicinski et al., 1996), whereas cyclin D1-nulls deleted exons I, II and III of the *cD1* gene (Sicinski et al., 1995) (both lines on C57BL/6 background). Breeding pairs (*cD2*$^{+/-}$ × *cD2*$^{+/-}$) were placed in mating cages at 17.00 and separated the next morning, designated embryonic day 0 (E0). BAC transgenic mice (C57BL/6) expressing enhanced green fluorescent protein (eGFP) driven by the *GAD67* (*Gad1* – Mouse Genome Informatics) promoter (Ango et al., 2004) were interbred with *cD2*$^{+/-}$ mice to produce *cD2*$^{+/+}$*::GAD67*^{eGFP} and *cD2*$^{-/-}$*::GAD67*^{eGFP} offspring.

[1]Department of Neurology and Neuroscience, Weill Cornell Medical College, New York, NY 10065, USA. [2]Department of Psychiatry, College of Physicians and Surgeons, Columbia University and [3]The New York State Psychiatric Institute, New York, NY 10032, USA. [4]Department of Neurosurgery, Weill Cornell Medical College, New York, NY 10065, USA.

*Author for correspondence (e-mail: mer2005@med.cornell.edu)

Accepted 31 August 2007

Immunohistochemistry and immunofluorescence

Immunohistochemical stains for all genotypes were processed in parallel to control for inter-experiment variability. For adult tissues: brains transcardially perfused [4% paraformaldehyde (PFA) in 0.1 M phosphate buffer (PB); for GABA immunofluorescence, 4% PFA with 0.025% glutaraldehyde, pH 7.4] were postfixed in 4% PFA for 1 hour. For embryonic tissues: embryonic brains were dissected free and drop-fixed in 4% PFA overnight at 4°C. Adult and embryonic tissue was processed for paraffin embedding (Tissue Tek 2000, Miles Laboratories). Brains were sectioned coronally at 4 or 10 μm (embryo and adult, respectively) and mounted on adhesive-coated slides (Fisher Scientific), deparaffinized and antigen retrieved in Reveal (Biocare Medical). Primary antibodies for DAB immunohistochemistry included: anti-somatostatin (α-SSN; MAB354, Chemicon International; 1:100), anti-parvalbumin (α-PV; 235, Swant; 1:100,000), anti-calbindin (α-CB; C9848, Sigma; 1:50,000), anti-calretinin (α-CALR; AB1550, Chemicon; 1:5000), anti-neuropeptide Y (α-NPY; Peninsula Laboratories; 1:24,000), anti-vasoactive intestinal peptide (α-VIP; Peninsula; 1:5000), anti-cyclin D2 (α-cD2; AB-4, Lab Vision; 1:1000), anti-cyclin D1 (α-cD1; SP4, Lab Vision; 1:5000), anti-Ki67 (α-Ki67; SP6, Lab Vision; 1:1000), anti-BrdU (α-BrdU; RPN20EZ, Amersham; 1:50), anti-phosphohistone H3 (α-PH3; 16-189, Upstate Biotechnology; 1:1000), anti-p27 (α-p27; P2092, Sigma; 1:10,000), anti-phosphorylated (ser 807/811) retinoblastoma (α-pRb; 9308, Cell Signaling Technologies; 1:200), anti-p57 (1:2000; Novus), anti-Nkx2.1 (Lab Vision; 1:300) and anti-Mash1 (BD Pharmingen; 1:1000). Sections were incubated in primary antibody, then in Signet Murine or Rabbit Linking and USA-HRP labeling reagents (Signet Laboratories). After α-SSN or α-CALR incubation, sections were incubated for 30 minutes each in goat anti-rat IgG or rabbit anti-goat IgG (1:200 in PB containing 0.1% BSA and 0.25% Triton X-100) and avidin-biotin-peroxidase complex (Vectastain Elite Kit; 1:100 in PB; Vector Laboratories). Bound immunoperoxidase was visualized with 3,3′-diaminobenzidine in hydrogen peroxide (Signet Laboratories) for 3-6 minutes.

Dual-labeled tissues were incubated in primary antibodies against: (1) GABA (A2052, Sigma; 1:1000) and PV (Swant; 1:50,000); (2) BrdU (Amersham; 1:50) and PH3 (Upstate; 1:1000); (3) BrdU (Amersham; 1:50) and Ki67 (Lab Vision; 1:1000); (4) anti-Tuj1 (Tubb3) (Covance; 1:2000) or anti-NeuN (Neuna60) (Chemicon; 1:4000), and either α-cD1 or α-cD2 at 4°C for 16 hours. Sections were washed in PB and incubated in Alexa Fluor-conjugated secondary antibodies (1:500, Invitrogen) for 1 hour, washed, and coverslipped with Vectashield with DAPI (Vector Laboratories). Sections were photographed digitally at 4×, 10× and 20× magnification using a SPOT camera (Diagnostic Instruments).

Immunohistochemistry for stereology

Brains were perfused and postfixed for 1 hour in 4% PFA in PB, cryoprotected overnight in 30% sucrose (in PB) and sectioned by sliding microtome (40 μm). One section per 200 μm throughout the forebrain was immunostained with αPV and αSSN as described above. In GAD67-eGFP+ mice, sections were incubated in a rabbit anti-GFP (α-GFP) antibody (Molecular Probes; 1:2000) and processed using αPV as above.

Quantitative stereology

PV, SSN or GAD67-GFP neuron numbers and density were obtained by two-dimensional and stereologic counting methods, using a Zeiss (Oberkochen, Germany) Axioplan2 microscope with internal Z drive fitted with a Ludl XY motorized stage and digital video camera (MicroBrightField), interfaced with Stereoinvestigator (MicroBrightField). Interneurons were counted in three brain regions: the hippocampal formation, somatosensory cortex (S1, barrel field) and motor cortex (M1, M2). (1) Hippocampus. Because of the non-random distribution of hippocampal PV+ and SSN+ interneurons, all immunoreactive interneurons were counted in the entire series of sections (one 40 μm section per 200 μm) throughout the rostrocaudal extent of the hippocampus. Laminar and regional boundaries were used as previously defined (Paxinos and Franklin, 2001). The total number of pyramidal neurons in the hippocampus was stereologically estimated and the volume of this lamina, as well as that of the granular layer of the dentate gyrus, was measured. Optical dissector frames and counting grids of 30 and 250 μm^2 were used. (2) Neocortex. The numbers of neocortical PV+ and SSN+ interneurons were determined using an unbiased stereologic method called the optical fractionator (West et al., 1991). Neocortical immunolabeled neurons were counted in two subregions within each area that included superficial (layers II and III) or deep (below layer III) cortical layers. The numbers of immunoreactive interneurons and of counterstained neurons, as assessed by morphological criteria that characterize the neuronal nuclei (Peters et al., 1991; Vaughan, 1984), were stereologically estimated in the cortex. The barrel field region of the somatosensory cortex was analyzed in each section of the series in which it was present, whereas the motor cortex was analyzed in 1 of every 2 sections in the series. Optical dissector frames and counting grid sizes of 30 and 250 μm^2 or 100 and 200 μm^2 were used to estimate neuronal or immunolabeled interneuron numbers, respectively, in the somatosensory cortex.

Optical dissector frames and counting grid sizes were chosen to permit systematic random sampling of three to five neurons within an 8 μm depth focusing range for each sampling field and more than 200 total neurons for each subregion within each case. Intra-sample coefficients of error (CE) (Schmitz and Hof, 2000) were always less than 0.05 and were equivalent across genotypes. All regions were sampled at 63× magnification in Koehler illumination conditions. The volume of the different laminar domains of interest in each subregion was estimated using the Cavalieri principle. The estimated total interneuron numbers were expressed as the density per subregion, thereby controlling for the reduced brain volume in *cD2*$^{-/-}$ mice. A Student's *t*-test was performed (significance $P<0.05$).

BrdU birthdating

Pregnant dams received BrdU (50 mg/kg) i.p. at E13.5 or E14.5-15.5. Brains from wild-type and *cD2*$^{-/-}$ littermates were harvested at P21, paraffin-embedded and processed to co-immunolabel BrdU and PV or SSN. PV and SSN neurons that were BrdU-labeled or unlabeled were counted in the 10× field of view of the somatosensory cortex (barrel fields; layers II-III). The proportion of BrdU+, PV or SSN+ neurons was calculated, averaging three sections/region for each case, and compared (Student's *t*-test; significance $P<0.05$).

Distribution of mitotic figures and BrdU index

Mice received BrdU (50 mg/kg) i.p. 1 hour prior to brain harvest. To calculate the proportion of S-phase cells in the ventricular zone (VZ) and SVZ, PH3 and BrdU double-labeled sections were photographed at 20× and both channels, in addition to DAPI, were merged in Adobe Photoshop. To determine the distribution of PH3-labeled M-phase cells, a 100×10 μm reticule was positioned centrally at the crest of the rostral MGE and PH3 or all BrdU/DAPI-labeled nuclei were counted. The VZ and SVZ abventricular boundary was estimated at 75 μm (Bhide, 1996), confirmed by the distribution of PH3+ cells. Three sections were averaged for each case. The labeling index was the proportion of DAPI-labeled cells in either region that were BrdU+. The entire MGE was photographed at 20× and montaged, if necessary, so that the rostral MGE from the interganglionic sulcus to the preoptic area was visible. The MGE was divided into dorsal and ventral halves from the midpoint of the crest of the MGE and the SVZ/VZ division was estimated as above. All labeled nuclei were counted, averaging three sections for each case. The SVZ/VZ ratio was calculated. Group means were compared (Student's *t*-test; significance $P<0.05$).

Quiescent (Q) and proliferative (P) fractions

Mice were BrdU-injected (50 mg/kg) at E13.5, for brain harvest at E14.5. The Q and P fractions were calculated from Ki67 and BrdU dual-labeled 4-μm paraffin sections, photographed at 20×. BrdU+ cells were counted in Adobe Photoshop using a 100×10 μm reticule positioned centrally at the crest of the rostral MGE. The channels were merged and the dual BrdU+Ki67-labeled nuclei were counted. Three MGE sections were sampled and averaged for each case. The P fraction was the proportion of all BrdU-labeled cells that were Ki67-immunoreactive. The Q fraction was the remaining proportion of BrdU single-labeled cells. Fractions were averaged for each group and means were compared using a Student's *t*-test (significance $P<0.05$).

Whole-cell voltage clamp recordings

Sex-matched *cD2*-null and wild-type littermates were recorded in the same session and the order of recording was counterbalanced across genotype. Cortical slices were prepared from ketamine/xylazine (90/10 mg/kg)-

anesthetized mice, aged 3-4 weeks. The brain was quickly removed into a cold high-glucose buffer containing 100 mM D-glucose, 75 mM NaCl, 2.5 mM KCl, 26 mM $NaHCO_3$, 1.25 mM NaH_2PO_4, 0.7 mM $CaCl_2$, 2 mM $MgCl_2$. Forebrain slices were cut coronally at 400 μm on a Vibratome (Camden Instruments), then perfused (1 ml/minute) for 30 minutes with an oxygenated (95% O_2, 5% CO_2) lactate buffer. For an additional hour, slices were perfused with oxygenated artificial cerebral spinal fluid (aCSF): 124 mM NaCl, 3 mM KCl, 26 mM $NaHCO_3$, 1.25 mM NaH_2PO_4, 2 mM $CaCl_2$, 1 mM $MgSO_4$, 10 mM D-glucose. Prior to recording, each slice was transferred to the recording chamber, maintained at 25 (±1)°C, and perfused with the oxygenated aCSF at 1-3 ml/minute with a gravity-fed system. Exchange of the bath by gravity occurred within 1 minute, and recordings began no sooner than 5 minutes after exchange of the perfusion solution.

Whole-cell voltage-clamp recordings were made with borosilicate pipettes (3-7 MΩ tip resistance) filled with: 300 mM CsCl (to block potassium conductances), 1 mM QX-314 Cl^- (to block sodium conductances), 2 mM $MgCl_2$, 0.1 mM $CaCl_2$, 10 mM HEPES, 1 mM EGTA, 2 mM ATP-Na_2, 0.1 mM GTP-Na_2, pH 7.3. To isolate miniature inhibitory postsynaptic currents (mIPSCs) mediated via $GABA_A$ chloride channels, the following drugs were added to the perfusion fluid: tetrodotoxin (TTX, 1.0 μM) to block impulse-dependent neurotransmitter release; (±)2-amino-5-phosphonopentanoic acid (50 μM) and 6,7-dinitroquinoxaline-2,3-dione or 6-cyano-7-nitroquinoxaline-2,3-dione (CNQX, 40 μM) to block fast glutamate-gated conductances. The holding potential of –70 mV and high internal [Cl^-] produced inward postsynaptic currents (PSCs). Complete blockade of spontaneous PSCs by the addition of gabazine (20 μM) to the perfusion fluid confirmed their mediation by $GABA_A$ chloride channels. Pyramidal neurons in frontal or frontoparietal cortex were impaled with pipettes connected via a Ag/AgCl wire to the headstage of an AxoClamp 2B amplifier (Axon Instruments, Foster City, CA). Corrections for liquid junction potentials were made offline. Series resistances were 20-40 MΩ and were compensated offline to avoid adding excessive baseline noise. Data were collected as Igor Pro (WaveMetrics, Lake Oswego, OR) '*.wav' 5-second, 1024-bit sweeps. Sweeps collected over a 2-5 minute period were concatenated and converted to an Axon Binary File using ABF Utility software (Synaptosoft, Leonia, NJ); MiniAnalysis software (Synaptosoft) was used to detect inhibitory IPSCs as events having rise time, amplitude and decay times significantly different from noise determined from periods in the trace apparently free from mIPSCs. Total mIPSC frequency and mIPSC amplitude frequency distributions were calculated. The effect of *cD2* genotype on mIPSC frequency was determined using a Student's independent *t*-test [(df=11)>4, two-tailed $P<0.001$].

Telemetry-based EEG recording

Mice anesthetized with ketamine/xylazine received two electrodes screwed into the skull and connected via AgCl wire to a transmitter (Data Science International) implanted under the skin near the shoulder. After 48 hours of recovery from surgery, mice were housed in conventional polycarbonate cages placed on top of receivers (Data Science International) that amplified the signal, which was digitized and stored on a PC running custom-written MathLab/Visual C++ routines. Recordings were collected for 18 hours. To detect seizures and count electrographic events, raw EEG data were band-pass filtered (3-70 Hz). Power spectral EEG analysis detected and quantified differences in cortical activity between wild-type and $cD2^{-/-}$ siblings for artifact-free, randomly chosen 10-second epochs. The frequency component of the fast-fourier transform of each EEG was binned at 25 Hz resolution for 100 epochs of 10 seconds (1000 seconds) and normalized within each animal. The effect of *cD2* genotype on EEG was determined using a parametric two-tailed *t*-test.

RESULTS

Cyclin D2 is required to produce the normal complement of PV interneurons

Although microcephalic, no subpopulation of neurons appears disproportionately affected in $cD1^{-/-}$ brain (Ciemerych et al., 2002; Sicinski et al., 1995). $cD2^{-/-}$ mice are also microcephalic (see Fig. S1 in the supplementary material). As specific interneuron deficits occur in $cD2^{-/-}$ cerebellum (Huard et al., 1999), the present study examined whether specific interneurons are lost in $cD2^{-/-}$ cortex. Two of the most prevalent interneuron subtypes, PV- and SSN-expressing, were compared between wild-type (WT) and $cD2^{-/-}$ cortex (Fig. 1). In $cD2^{-/-}$, PV neuron numbers were reduced in neocortex, especially in superficial layers (Fig. 1A,B), and were also reduced in the $cD2^{-/-}$ hippocampus (Fig. 1C,D). Stereologically determined density measurements of interneuron subtypes in the hippocampus, somatosensory and motor cortex, allowed for normalization of the impact of microcephaly. The density of PV interneurons was reduced by 40% in the $cD2^{-/-}$ hippocampus and by 30% in somatosensory and motor cortices relative to WT (Fig. 1E). The mean diameter measurements for PV interneurons were unchanged, indicating no sampling artifact. The SSN cell density in $cD2^{-/-}$ cortex did not differ from WT (Fig. 1G). In hippocampus, the SSN interneuron density was slightly elevated in the stratum oriens of $cD2^{-/-}$ mice (Fig. 1H-J). The density of all Nissl-labeled neurons, identified by the appearance of their chromatin, was also stereologically sampled in somatosensory cortex and there were no differences in packing density in $cD2^{-/-}$ mice compared with WT (see Fig. S2 in the supplementary material). The $cD2^{-/-}$ cortex was thinned overall, but was substantially thinner superficially [42% (layers I-III) versus 31% (layers IV-VI) reduction from WT], and this was equally true for *cD2*- and *cD1*-null mice. Despite accounting for reduced volume, the reduction in density of PV interneurons remained more pronounced in superficial cortical layers (~45-50% reduction in layers I-III versus 20-30% reduction in layers IV-VI, compared with WT). Thus, adult $cD2^{-/-}$ mice display selective reductions in the PV interneuron subtype, particularly in superficial layers.

Interneuron reductions in $cD2^{-/-}$ may result from defective cell production or survival. PV expression only reaches adult levels in the third postnatal week. PV+ neuron numbers were already reduced at P25 in $cD2^{-/-}$ (see Fig. S3A,B in the supplementary material). Whether decreased PV interneuron density is a general feature of microcephaly was explored. Owing to their diminished lifespan, $cD1^{-/-}$ versus WT littermates were examined at 5-6 weeks of age. Whereas PV neuron density was reduced in the $cD2^{-/-}$ cortex (see Fig. S3C,D in the supplementary material), the pattern in $cD1^{-/-}$ was indistinguishable from WT (see Fig. S3E,F in the supplementary material). $cD1^{-/-}$ mice similarly showed no differences in SSN neuron density or distribution (see Fig. S3G,H in the supplementary material). Microcephalic $cD1^{-/-}$ mice also had thinner superficial cortical layers (see Fig. S2 in the supplementary material). Therefore, the selective PV interneuron deficit in $cD2^{-/-}$ mice is not a general feature of microcephaly or of deficient late-progenitor divisions. There was no sign of increased apoptosis by TUNEL or caspase-3 labeling in the $cD2^{-/-}$ MGE or cortex (see Fig. S4 in the supplementary material). Thus, cD2 loss causes disproportionate deficits in PV interneuron generation.

Reductions in PV immunolabeling reflected cell loss, not simply a decrease in PV expression (Fig. 2). The PV subpopulation constitutes approximately 50-60% of all interneurons and, therefore, the lower GABA neuron density due to decreased PV+ neurons in the $cD2^{-/-}$ mouse would be predicted to comprise a reduction of about 15%. Only minor differences in the total GABA+ neuropil and neuronal number were evident qualitatively in $cD2^{-/-}$ as compared with WT cortex (Fig. 2A,E). These differences corresponded to reduced PV immunofluorescence in *cD2* nulls, as compared with WT (Fig. 2B,F). Most GABA-immunoreactive cells in the cortex contained PV; however, the number of GABA-positive PV-negative cortical neurons was not substantially increased in *cD2* nulls (Fig. 2C,G). Thus, the reductions in PV neuron numbers in $cD2^{-/-}$ mice

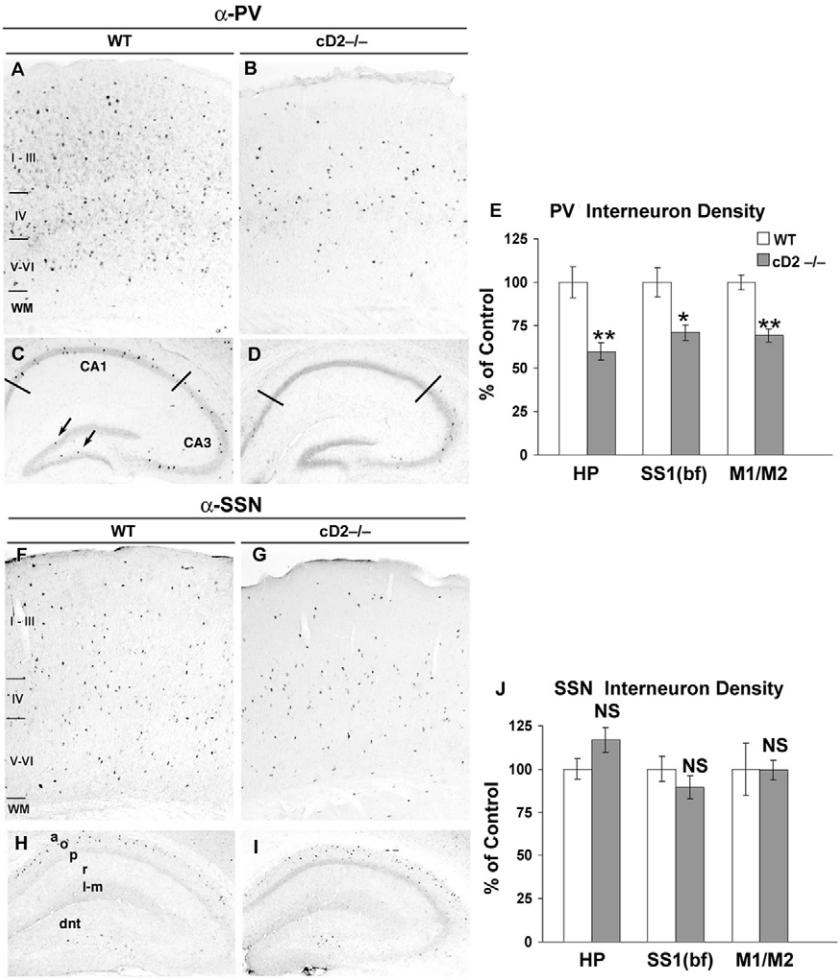

Fig. 1. Parvalbumin (PV) and somatostatin (SSN) immunoreactivities in somatosensory cortex and hippocampus of wild-type and *cD2*$^{-/-}$ mice. (**A**,**B**) PV neurons are especially reduced in superficial cortical layers in *cD2*$^{-/-}$. (**C**,**D**) Hematoxylin-counterstained sections show PV interneurons are reduced in the *cD2*$^{-/-}$ hippocampus. (**E**) PV neuron density is reduced in all regions of *cD2*$^{-/-}$ cortex (HP>SS1, M1/M2). (**F**,**G**) The relative SSN neuron density distribution is similar in WT and *cD2*$^{-/-}$ nulls despite cortex thinning. (**H**,**I**) The density of SSN-immunolabeled neurons is slightly increased in the hippocampal stratum oriens and dentate of *cD2*$^{-/-}$. (**J**) The SSN neuron density is unchanged in *cD2*$^{-/-}$ mice. (A-D,F-I) 40 μm sections. a, alveus; o, stratum oriens; p, stratum pyramidale; r, stratum radiatum; l-m, lacunosum moleculare layer; dnt, dentate gyrus; HP, hippocampus; SS1(bf), primary somatosensory cortex (barrel field region); M1/M2, primary and secondary motor cortex; WT, wild type. Mean±s.e.m. densities of PV-IR neurons in the null are expressed as percentage of control (WT). *n*=5-8 per genotype per region; *, *P*<0.02; **, *P*<0.001.

are reflected in overall numbers of GABAergic neurons. To further explore the specificity of this loss, a *GAD67* promoter-driven eGFP BAC transgenic mouse (Ango et al., 2004) was crossed with *cD2*$^{+/-}$ mice. In the GAD67-eGFP transgenics, a subpopulation of medium and large PVergic interneurons can be identified by their expression of GFP. Numbers of GFP-immunoreactive neurons were reduced in *cD2*$^{-/-}$*::GAD67*^{eGFP} mice compared with *cD2*$^{+/+}$*::GAD67*^{eGFP} (Fig. 2I,J), and the eGFP+ density differences in the cD2-deficient double mutants were identical to the PV-immunolabeled estimates (see Fig. S5 in the supplementary material). Therefore, GABAergic interneurons are truly lost in *cD2*$^{-/-}$ and deficits are not attributable to an isolated loss of PV expression.

Additional interneuron subtypes were examined in *cD2*$^{-/-}$ and WT sections immunolabeled for CB, CALR, NPY and VIP (see Materials and methods). There were no immunolabeling differences between *cD2*$^{-/-}$ and WT for any of these interneuron subgroups (see Fig. S6 in the supplementary material). Furthermore, the superficial laminae, where the reductions in PV+ interneurons were greatest, contained normal distributions of CB+, CALR+, NPY+ and VIP+ interneurons. The data support an important role for cD2 in the generation of PV interneurons.

Reduced synaptic inhibition and increased irritability in the *cD2*-null cortex

PV+ GABAergic interneurons form inhibitory synapses primarily onto perisomatic compartments of pyramidal neurons in the hippocampus (Freund and Buzsaki, 1996) and neocortex (Kawaguchi and Kubota, 1998; Wang et al., 2002). In previous studies, the frequency of GABA-mediated mIPSCs in hippocampal pyramidal neurons correlated with the density of GABAergic synapses (Hartman et al., 2006; Swanwick et al., 2006). Thus, if the decreased density of PV+ GABAergic interneurons led to a significant decrease in the density of their GABAergic synapses, we would observe a reduction in mIPSC frequency in cortical pyramidal neurons. Whole-cell voltage-clamp recordings were used to isolate and quantify $GABA_A$ receptor-mediated mIPSCs in frontal cortical pyramidal neurons in slices from *cD2*$^{-/-}$ mice and their matched WT littermates. Cortical pyramidal neurons exhibited spontaneous inward currents (Fig. 3A) with modal rise and decay times of 4 and 18 milliseconds, respectively. The rise and decay times of these events were consistent with a perisomatic origin of the events (Swanwick et al., 2006). The amplitude frequency distribution (Fig. 3B) showed that the majority of mIPSCs recorded across all mice had amplitudes of 2-30 pA, with rarer events of up to 60 pA. These currents were completely blocked by the presence of the $GABA_A$ receptor antagonist gabazine in the bath (data not shown). The mean frequency of $GABA_A$-mediated mIPSCs was significantly reduced in *cD2* nulls (Fig. 3C) (*P*<0.001). Thus, the reduction in PV+ interneurons in *cD2* nulls, as quantified in the anatomical experiments, is associated with a significant decrease in $GABA_A$-mediated inhibitory synaptic activity at cortical projection neurons.

The distribution of the mean normalized power spectral density (nPSD) of telemetry-based EEG differed significantly between *cD2*$^{-/-}$ and WT mice (Fig. 3D-F) (*P*<0.05). In this example, the *cD2*$^{-/-}$ animal

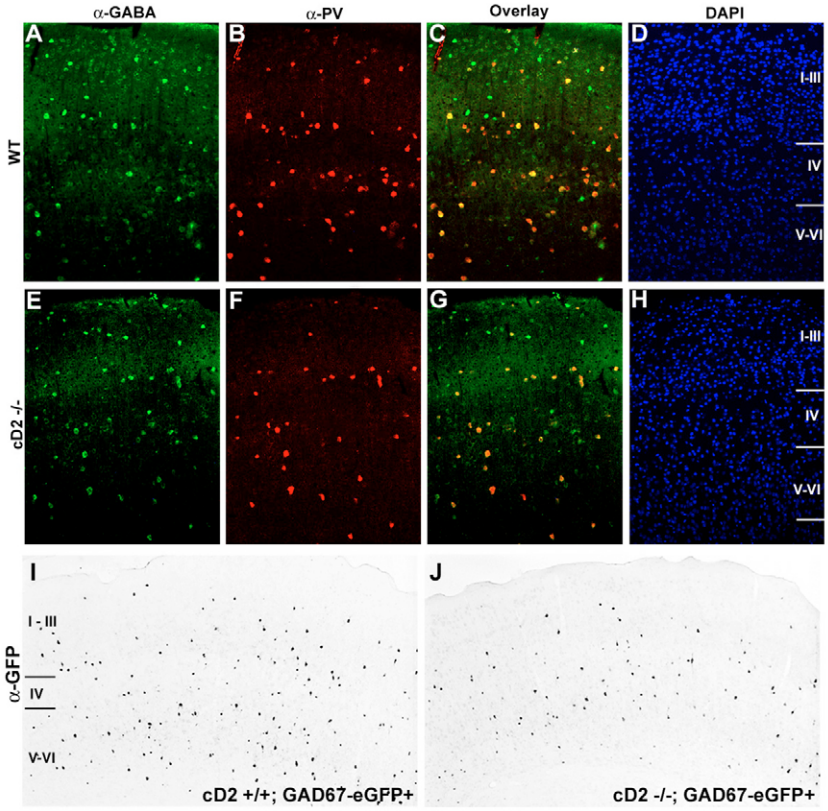

Fig. 2. Co-localization of γ-aminobutyric acid (GABA) and PV in somatosensory cortex. (**A-D**) Adult WT and (**E-H**) *cD2*$^{-/-}$ mice. Sections, 10 μm. GABA+ (A,E) and PV+ (B,F) neurons and processes are distributed in all layers of the cortex and GABA-immunolabeled neuropil is moderately reduced in *cD2*$^{-/-}$ compared with WT. GABA and PV overlay images (C,G) show that most GABA+ cells in the cortex contain PV; however, GABA-immunolabeled, PV-negative cortical neurons are not substantially increased in *cD2*$^{-/-}$. (D,H) The GABA- and PV-immunolabeled neuropil are most substantially reduced in the superficial cortical lamina. (**I**,**J**) In 40 μm sections, GFP-immunoreactive neuron numbers are reduced in *cD2*$^{-/-}$*::GAD67*^{eGFP} mice compared with *cD2*$^{+/+}$*::GAD67*^{eGFP} (see Fig. S5 in the supplementary material). Therefore, GABAergic neurons are truly lost in *cD2*$^{-/-}$ mice.

exhibited higher spectral power over 200-300 Hz, whereas the WT animal exhibited higher spectral power over the 1-100 Hz range. The dominant peak was shifted toward higher frequencies in the *cD2*-null animal (P<0.05). These results indicate enhanced cortical excitation in nulls compared with WT mice.

Cell cycle regulation within the MGE is disturbed in *cD2*$^{-/-}$ mice and contrasts with *cD1*$^{-/-}$

Cortical and hippocampal PV and SSN interneuron subtypes are produced primarily in the MGE, whereas VIP and NPY subtypes originate primarily in the caudal GE (Butt et al., 2005; Xu et al., 2004). Proliferation and cell survival within the MGE were explored in *cD2*$^{-/-}$ embryos as potential mechanisms resulting in PV interneuron deficits.

Cyclins D1 and D2 have distinct expression patterns in the embryonic forebrain with limited overlap (Glickstein et al., 2007). cD1 cells are mainly localized to the ventricular zone (VZ), whereas cD2-labeled cells are more prevalent in the SVZ (Fig. 4A,B). Whereas cD1 labeling was uniform in the VZ, cD2 appeared more robust in the dorsal lateral ganglionic eminence (LGE) and ventral MGE, SVZ and VZ. Very few MGE nuclei co-express cD1 and cD2 (Glickstein et al., 2007). Each cyclin, therefore, appears to have distinct regional control of proliferation in the GE. The expression of cD1 does not compensate for cD2 in the *cD2*$^{-/-}$ SVZ (Fig. 4C). By contrast, *cD1*$^{-/-}$ mice display cD2-immunolabeling that is enhanced in the VZ and is present in the SVZ of the entire GE (Fig. 4D). Thus, cD2 compensates for cD1 loss in the VZ of *cD1*$^{-/-}$ mice, but cD1 is not induced in the SVZ of the *cD2*$^{-/-}$ MGE. This difference in cyclin expression is reflected in the expression of genes governing interneuron specification, *Nkx2.1* and *Mash1* (also known as *Ascl1* – Mouse Genome Informatics) (Fig. 4E-J) (Marin et al., 2000). Whereas the area of Nkx2.1 and Mash1 labeling is reduced in the *cD2*$^{-/-}$ MGE, their expression is preserved or expanded in the *cD1*$^{-/-}$ MGE that induces cD2.

Two G1-S regulatory proteins, the cyclin-dependent kinase inhibitor p27 and phosphorylated (ser807/811) retinoblastoma (pRb), were examined in the MGE in *cD2*$^{-/-}$ and *cD1*$^{-/-}$and WT littermates (Fig. 5). The absence of p57 (also known as p57Kip2 and Cdkn1c – Mouse Genome Informatics) labeling in the MGE-VZ/SVZ at E12 and E14.5 suggested the selective importance of p27 in the MGE at these ages (see Fig. S7 in the supplementary material). Compared with WT embryos, p27 immunoreactivity was elevated in *cD2*$^{-/-}$ sections (Fig. 5A,B,E,F), whereas pRb-immunolabeling was reduced, especially in the *cD2*$^{-/-}$ SVZ (Fig. 5D,H). The increased expression of p27 and decreased expression of pRb in *cD2*$^{-/-}$ MGE were consistent with slower progression through G1 phase in the absence of cD2. By contrast, p27 immunoreactivity was dramatically reduced in the *cD1*$^{-/-}$ VZ and increased in the SVZ (Fig. 5J,N), as compared with either WT littermates (Fig. 5I,M) or *cD2* nulls. pRb was somewhat increased in the *cD2*$^{-/-}$ VZ, but levels were equivalent in the SVZ of WT (Fig. 5K,O) and *cD1*$^{-/-}$ (Fig. 5L,P) GEs. The overexpression or knockdown of Rb and p27 has selective effects on cell cycle duration in G1–S phase (Ferguson and Slack, 2001; Ferguson et al., 2002; Mitsuhashi et al., 2001; Sherr, 2000). Therefore, these immunolabeling results indicate that cyclins D1 and D2 are poised to differentially regulate the cell cycle progression, and removal of either cyclin has distinct effects on MGE proliferation. Moreover, cD2 might have a specific role in the formation of the SVZ and in the proliferation of its progenitors.

Proliferation within the VZ or SVZ and cell cycle exit were compared in *cD2*$^{-/-}$, *cD1*$^{-/-}$ and WT MGE. In embryos lacking cD2, PH3 M-phase nuclei had a similar distribution in the GE and this was abbreviated in depth in the SVZ (Fig. 6B,F). Ki67 labeling (S–G2–M-phase cells) in the VZ was reduced in its extension into the SVZ in *cD2* nulls (Fig. 6C,D,G,H). Thus, the proliferating progenitor pool was diminished in the *cD2*$^{-/-}$ SVZ, or the G1 phase

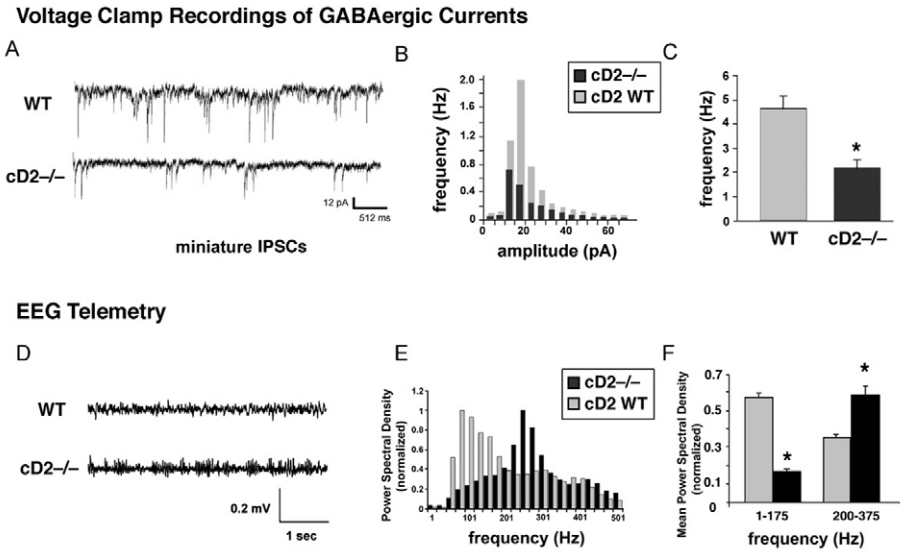

Fig. 3. Consequences of PV-interneuron loss in *cD2*$^{-/-}$ brain. (**A-C**) Whole-cell voltage-clamp recordings in acute slices show $GABA_A$ receptor-mediated miniature inhibitory postsynaptic currents (mIPSCs) in frontal cortical pyramidal neurons. (A) Example traces under conditions isolating $GABA_A$ receptor-mediated mIPSCs (see text). (B) Mean frequency distribution of mIPSC amplitudes in *cD2* mutant (black) and WT (gray) neurons. (C) Average frequency of mIPSCs of all amplitudes. *, *cD2* nulls<WT, $P<0.05$. (**D-F**) Cortical electroencephalographic (EEG) recorded by telemetry from awake-behaving mice. (D) Example traces for cyclin *cD2*$^{-/-}$ and WT siblings show intermittent bursts of faster frequency discharges in the *cD2* null. (E) Mean normalized power spectral density (nPSD) distribution over 1000 seconds, collected in randomly selected blocks of 10 seconds each in *cD2* mutant (black) and WT (gray) with 25 Hz bin resolution. (F) Average of mean nPSD of EEG for low (1-175 Hz) and high (200-375 Hz) frequency. *, $P<0.05$, as compared with WT.

was significantly prolonged. By contrast, PH3 and Ki67 staining were indistinguishable between *cD1*$^{-/-}$ and WT littermates (Fig. 6I-L), indicating that normal density but reduced total numbers of interneurons in these mutants most likely results from fewer overall cell divisions or a survival defect that uniformly affects the MGE. TUNEL and activated caspase-3 immunolabeling revealed no differences between WT and *cD2*$^{-/-}$ GE at E12, E14.5, or in cortex at E17, P3, P7 or P14, refuting apoptosis in the *cD2*$^{-/-}$ GE as a mechanism contributing to interneuron deficits (see Fig. S4 in the supplementary material).

Cell cycle dynamics were examined (Fig. 7). Numbers of PH3-labeled M-phase nuclei were significantly reduced in both the VZ and the SVZ of *cD2* nulls (Fig. 7A) at E12.5 and E14.5. At E14.5, fewer BrdU pulse-labeled S-phase nuclei were present in the *cD2*-

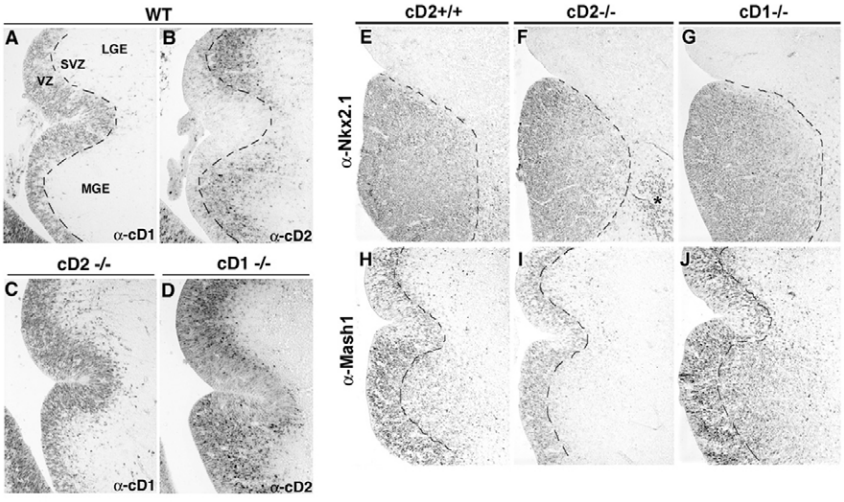

Fig. 4. Reciprocal cyclin D expression changes in *cD1*$^{-/-}$ or *cD2*$^{-/-}$ mice at E14.5. (**A-D**) The distribution of nuclei expressing cD1 or cD2 proteins is distinct and non-overlapping in the medial ganglionic eminence (MGE) at E14.5. Compared with WT (A,B), mice lacking cD2 (C) have as many cD1-immunoreactive cells in the VZ as WT MGE, but the SVZ has a few more cD1+ cells, partially compensating for loss of cD2. In mice lacking cD1 (D), cD2-immunoreactive nuclei are more prevalent in the VZ and are also observed in the deep SVZ to an extent similar to that in WT. (**E-G**) Compared with WT (E), Nkx2.1 expression in the E14.5 MGE is reduced in area in *cD2*-null mice (F), and the same or increased in *cD1*-null mice (G) (MGE perimeter bordered with dashed line). The asterisk denotes Nkx2.1 labeling in the mantle region that was present in all genotypes but more easily captured here owing to reduced MGE volume. (**H-J**) Compared with WT (H), Mash1 expression in the MGE is reduced in *cD2*-null SVZ (I) and enhanced in *cD1*-null SVZ (J) (dashed line demarcates the VZ/SVZ border).

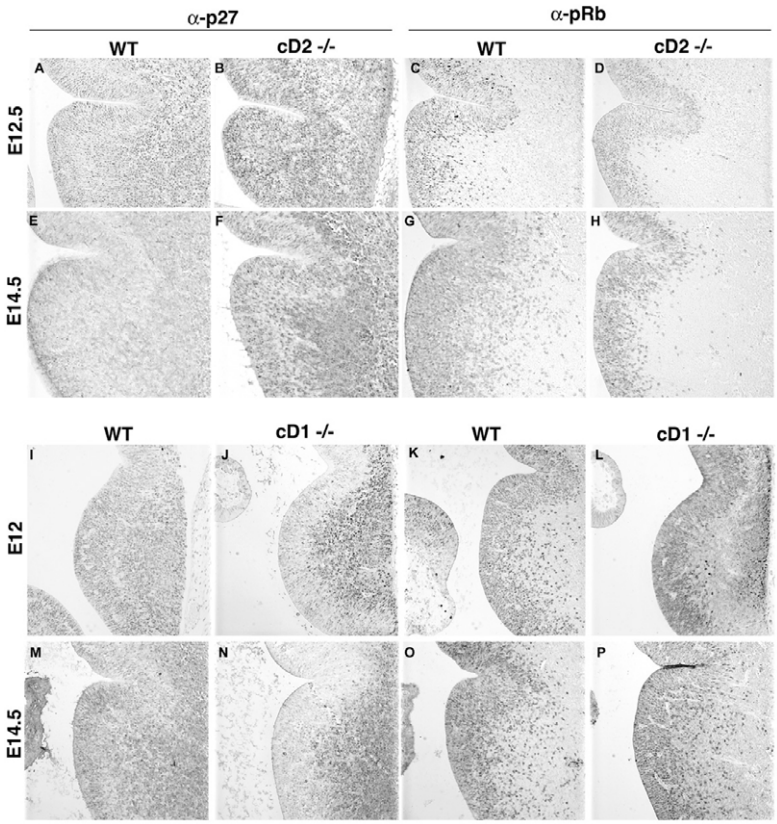

Fig. 5. Cdk-inhibitor p27 and cD-Cdk effector retinoblastoma in the MGE of *cD2*$^{-/-}$ and *cD1*$^{-/-}$ mice as compared with wild-type littermates. (**A-H**) At E12.5 (A-D) and E14.5 (E-H), the labeling-intensity of p27 (A,B,E,F) is increased and fewer nuclei label with phosphorylated Rb (pRb) (C,D,G,H) in *cD2*$^{-/-}$ mice than in the WT. (**I-P**) The distribution of p27+ cells is reduced specifically in the VZ of *cD1*$^{-/-}$ (J,N), as compared with WT (I,M). pRb labeling is equivalent in *cD1*$^{-/-}$ and WT MGE.

null SVZ compared with WT (Fig. 7B,C). The BrdU labeling index was unchanged in the VZ, but was significantly reduced by 57% in the *cD2*$^{-/-}$ SVZ (Fig. 7D) as compared with WT. The dorsoventral SVZ/VZ ratios of mitotic nuclei and of nuclei labeled by a 1-hour pulse of BrdU were compared in the MGE because of the suggestion that cD2 is more heavily expressed ventrally (Table 1). In WT MGE, the average numbers of S- or M-phase nuclei in the VZ or SVZ and the SVZ/VZ ratio did not significantly differ in the ventral, as compared with the dorsal, MGE. The SVZ/VZ ratios in *cD2*$^{-/-}$ MGE were, however, significantly reduced in both the dorsal and ventral

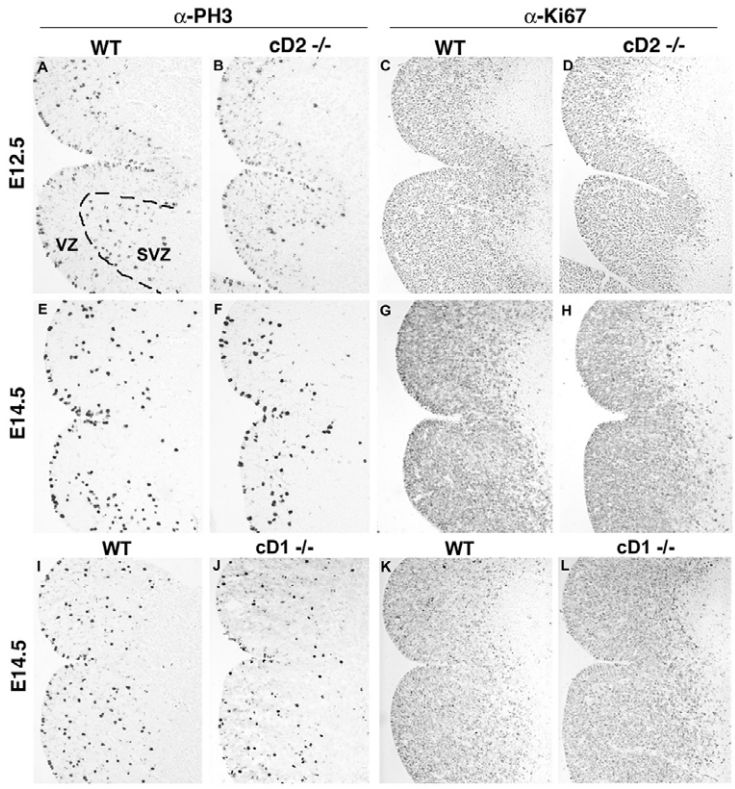

Fig. 6. Proliferation markers PH3 and Ki67 are altered in the MGE of *cD2*$^{-/-}$, *cD1*$^{-/-}$ and WT littermates. (**A**,**B**,**E**,**F**) The numbers of PH3-labeled M-phase nuclei are reduced in both the VZ and SVZ of *cD2*$^{-/-}$ mice. The distribution of PH3-immunolabeled nuclei is most substantially reduced in *cD2*$^{-/-}$ in the ventral SVZ. (**C**,**D**,**G**,**H**) The numbers and distribution of Ki67-immunoreactive nuclei are also reduced in the SVZ of *cD2*$^{-/-}$ as compared with WT. (**I**,**J**) The numbers and distribution of PH3+ nuclei in *cD1*$^{-/-}$ and WT are identical. (**K**,**L**) Distribution of Ki67+ nuclei is similar in WT and *cD1*$^{-/-}$. Proliferation in the VZ and SVZ of *cD1* nulls is less affected than in *cD2*$^{-/-}$ mice.

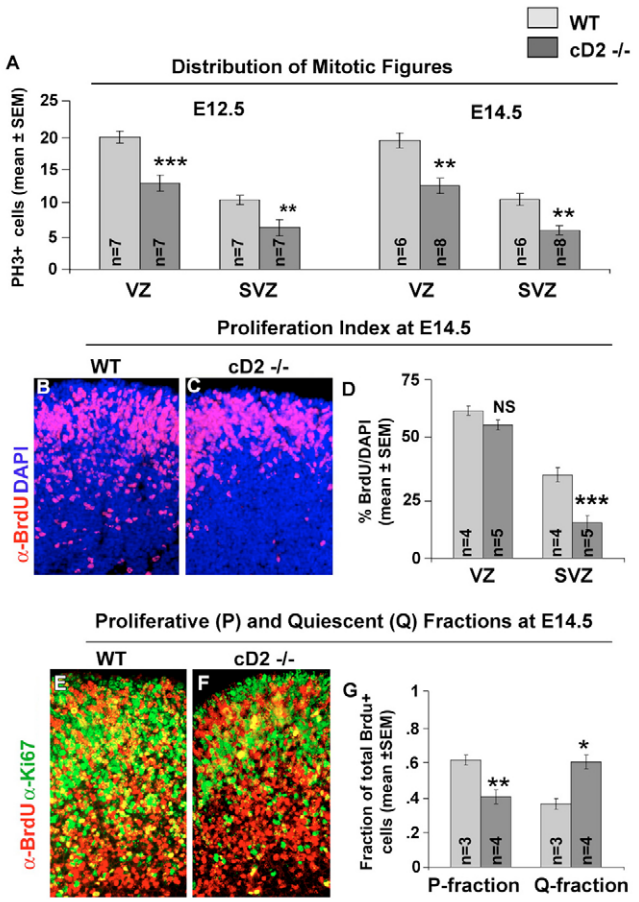

Fig. 7. Reduced proliferation and early progenitor cell cycle exit in *cD2*$^{-/-}$ MGE. All sections, 4 μm. (**A**) Fewer nuclei label with the M-phase marker PH3 in the VZ and SVZ of the *cD2*$^{-/-}$ MGE than in WT. (**B-D**) Fewer nuclei are labeled by a 1-hour BrdU pulse in *cD2*$^{-/-}$ (C) than WT (D) MGE. The proportion of total (DAPI) nuclei labeled by anti-BrdU is significantly reduced in the SVZ. (**E-G**) Dual-immunolabeling with BrdU and Ki67 (to label S-phase through M-phase cells) shows the total numbers of nuclei labeled by a 24-hour BrdU pulse is slightly reduced in *cD2*$^{-/-}$ MGE, but numbers of BrdU+ nuclei not co-labeled with Ki67+ are increased in the MGE of *cD2* nulls (F), as compared with WT (E). Quantification of dual (P fraction) and single (Q fraction; BrdU alone) labeled cells indicates a decrease in the proliferating, P fraction and a corresponding increase in the quiescent, Q fraction in *cD2*$^{-/-}$ MGE (G), suggesting progenitors are prematurely depleted in *cD2*$^{-/-}$ mice. *, $P<0.05$; **, $P<0.01$; ***, $P<0.003$.

MGE compared with WT, primarily as a consequence of significant reductions in the numbers of SVZ M- or S-phase labeled nuclei and the reductions were more marked (by 6-9%) in the ventral, than in the dorsal, MGE. These findings suggest a particular importance of cD2 in the ventral MGE. BrdU injection at E13.5 and harvest at E14.5 enabled calculation of the quiescent (Q) and proliferative (P) fractions, indicating the proportion of BrdU-labeled cells leaving or remaining, respectively, in the cell cycle during 24 hours. BrdU-labeled nuclei were slightly reduced in *cD2*$^{-/-}$; however, many fewer cells co-labeled with BrdU/Ki67 in *cD2* nulls than in WT (Fig. 7E,F). The P fraction was decreased by 34% in *cD2* nulls and the corresponding Q fraction was thus increased. Therefore, more progenitor cells at E14.5 exit the cell cycle in *cD2* nulls than in WT, which suggests premature terminal differentiation of progenitors in the absence of cD2. Consistent with the premature exit of progenitors from the cell cycle, Tuj1 immunostaining was increased in the *cD2*$^{-/-}$ SVZ, encroaching on the VZ, and the region of NeuN+ cells was expanded in the mantle zone, whereas Tuj1 and NeuN immunolabeling were both decreased in the *cD1*$^{-/-}$ embryos in which cD2 was induced (see Fig. S8 in the supplementary material).

Finally, whether early depletion of the progenitor pool in the *cD2*$^{-/-}$ MGE leads to the selective deficit in the PV interneuron population was examined using BrdU birthdating (Fig. 8A). Embryos received BrdU at either E13.5 or E14.5-15.5 and survived until brains were collected at P21 for dual-immunolabeling and quantification. The proportion of layer II-III PV interneurons that were also BrdU+ was significantly reduced in *cD2*-null cortex, whether cells were born early (E13.5, –39%) or late (E14.5-15.5, –53%). By contrast, the proportion of SSN neurons generated at any time did not differ between WT and *cD2*$^{-/-}$ littermates.

Four striking differences between the *cD2* and *cD1* knockouts emerge (Table 2). First, cD2 is significantly induced in the VZ of *cD1* nulls, whereas cD1 is only marginally increased, if at all, in the SVZ of *cD2* nulls. Second, cD2 induction in the *cD1*$^{-/-}$ VZ is accompanied by a marked suppression of p27 in the VZ, whereas p27 is upregulated in the SVZ of *cD2* nulls. Third, phosphorylated Rb is substantially decreased in the SVZ of *cD2*-null embryos. Fourth, this apparent increase in p27 and decrease in pRb in the *cD2*-null SVZ are together consistent with the increased Q fraction (proportion of cells exiting the cell cycle) over a 24-hour period in *cD2*$^{-/-}$ embryos. These results indicate significant distinctions between the regulation of cD2 and cD1 in developing brain and in how these two cyclins balance the proliferation of different progenitor pools.

Table 1. Analysis of M- or S-phase cells in the dorsal compared with the ventral MGE

PH3-labeled nuclei

	E12.5			E14.5		
	WT	*cD2*$^{-/-}$	Δ%	WT	*cD2*$^{-/-}$	Δ%
dSVZ/VZ	0.61±0.08	0.30±0.06*	–51	2.11±0.33	1.38±0.08*	–35
vSVZ/VZ	0.67±0.09	0.28±0.04†	–59	2.20±0.09	1.30±0.12†	–41
n	6	6		7	7	

BrdU-immunoreactive nuclei labeled by a 1-hour BrdU pulse at E14.5

	WT	*cD2*$^{-/-}$	Δ%
dSVZ/VZ	0.52±0.06	0.29±0.04*	–46
vSVZ/VZ	0.53±0.03	0.24±0.02†	–55
n	4	5	

*$P<0.05$.
$^{\dagger}P<0.005$.

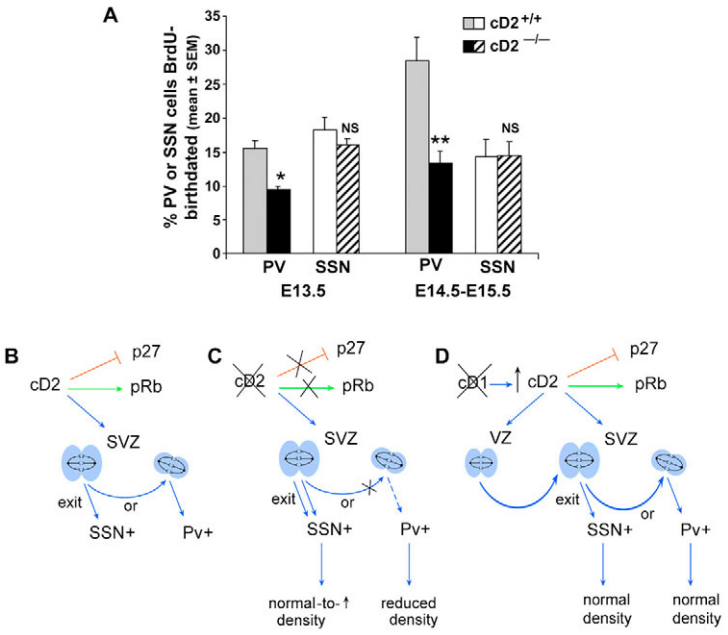

Fig. 8. Mechanism of PV loss in the *cD2*$^{-/-}$ MGE. (**A**) Deficits in PV interneuron production occur in early and late MGE populations. The proportion of PV+ cells in layer II-III somatosensory cortex that is also labeled by BrdU injected at E13.5 (n=2 per genotype) or E14.5-15.5 (n=5 per genotype) is significantly reduced in *cD2*$^{-/-}$ mice, whereas the proportion of SSN+ cells generated at any age is the same in *cD2*$^{-/-}$ and WT littermates. *, P<0.05; **, P<0.002. (**B-D**) Model of D cyclin roles in the MGE. cD2 normally suppresses p27 levels more strongly than does cD1, requiring more p27 to accumulate before cells can exit the cycle. cD2 also promotes phosphorylation of Rb (pRb), facilitating progression through G1 phase and perhaps influencing downstream gene transcription. cD2 support of SVZ divisions promotes the balanced production of SSN+ and PV+ interneurons. (C) In the absence of cD2, constraints on p27 are lifted and pRb levels fall, hastening cell cycle exit and leaving the proportion of SSN+ neurons unchanged or slightly increased, while disproportionately fewer PV+ interneurons are generated. (D) Loss of cD1 induces cD2 in the VZ, which inhibits p27 and promotes pRb. Divisions continue in both the VZ and SVZ, although they may be slower overall. This leads to fewer rounds of division and reduced total neuronal numbers, but preserved SSN+ and PV+ neuron densities in *cD1*$^{-/-}$ brains.

DISCUSSION

Stereological analyses reveal significant reductions in the density of PV, but not of SSN, -immunolabeled interneurons, in cerebral and hippocampal cortex. Both PV+ and SSN+ subtypes derive largely from the MGE, where cD2 is expressed in the majority of SVZ cells, especially those that are Olig2-negative as SVZ populations diverge toward glial and neuronal lineages (Glickstein et al., 2007; Xu et al., 2004; Xu et al., 2003). Although loss of either cD2 or cD1 results in smaller forebrains, only *cD2* nulls have disproportionately reduced neuronal subtypes in cerebellum (Huard et al., 1999), cortex and hippocampus (present report). Therefore, cD2 has an indispensable role in generating the normal proportion of particular neuronal subsets in developing brain.

Reduced spontaneous GABAergic currents and increased cortical irritability in *cD2*-null mice

Mice lacking particular subsets of interneurons are invaluable toward a deeper understanding of the specific role of these subsets in brain function. Selective interneuron reductions are known in three other mouse models. In *Dlx1*-null mice, reductions in somatostatinergic and calretinin interneurons result in spontaneous seizures (Cobos et al., 2005). In contrast to interneuron deficits in *cD2* nulls, interneuron losses in the *Dlx1* model have been attributed to a survival defect in the adult. Mice lacking uPAR have deficits in PV interneurons in the adult (but not juvenile) cerebral cortex and in SSN interneurons in hippocampus and they also suffer spontaneous seizures (Eagleson et al., 2005). In mice lacking the tailless gene (*Tlx*; now known as *Nr2e1* – Mouse Genome Informatics), the numbers of CALR and SSN interneurons are reduced, whereas the PV subtype is spared. *Tlx* mutants have reduced fear- and anxiety-related behavior; a seizure phenotype has not been reported (Roy et al., 2002). The interneuron deficit in *cD2*-null mice is unique in that it involves only PV+ interneurons, both in cortex and hippocampus. Moreover, PV interneuron deficits are detectable in *cD2*$^{-/-}$ mice at the earliest ages in which this interneuron phenotype has matured in cortex (3 weeks). Electrophysiological data presented here begin to characterize the functional consequences of interneuron deficits in *cD2*$^{-/-}$ cortex. Cortical projection neurons exhibit a decrease in the frequency of mIPSCs that are characteristic of perisomatic inhibitory synapses, a large proportion of which are PVergic (Kawaguchi and Kubota, 1998). Thus, the decreased density in PV interneurons in the *cD2* nulls has a significant impact on cortical inhibition. This is further evidenced by the increased frequency and amplitude of paroxysmal cortical discharges in the EEG of the awake-behaving *cD2*-null mouse. In addition, the shift in the dominant spectral power density peak toward higher frequencies in baseline recordings from *cD2* nulls is consistent with a loss of GABAergic tone or GABA content of the extracellular milieu resulting in the generation of ictal discharges.

Table 2. Cell cycle analysis of *cD1*$^{-/-}$ and *cD2*$^{-/-}$ MGE compared with WT

		BrdU (1-hour pulse)	p27	pRB	Q fraction (24 hour BrdU/Ki67)	cD1	cD2
cD1$^{-/-}$	VZ	↓*	↓↓	↔	↑↓†	0	↑↑
	SVZ	↔	↑↓	↔	↓†	0	↑
cD2$^{-/-}$	VZ	↔	↑	↓	↔	↑	0
	SVZ	↓↓	↑↑	↓↓	↑↑	↔	0

*Trend toward 15-20% reduction, not statistically significant (n=5 *cD1*$^{-/-}$ versus 3 WT).
†Indicated by increased Ki67 and equivalent BrdU labeling of *cD1*$^{-/-}$ versus WT littermates.

Cell cycle deregulation as a mechanism contributing to PV interneuron deficits

Reduced PV interneuron numbers may result from aberrant regulation of the cell cycle leading to reductions in proliferation in the SVZ and premature terminal differentiation of progenitor cells. Birthdating data presented here indicate that the proportion of PV (but not SSN) interneurons produced by the MGE is affected in *cD2*$^{-/-}$ brains throughout neurogenesis, but PV production deficits become more severe at later ages as the progenitor pool is depleted. That normal densities of other interneuron subtypes (e.g. CALR, VIP) are produced in *cD2*$^{-/-}$ mice suggests an MGE-specific requirement for cD2 in the genesis of PV interneurons.

The most direct model for cD2 involvement in histogenesis, supported by analyses here, is that this cyclin is both differently regulated and has a different impact on the cell cycle than cD1 in the MGE. Cyclin D1/D2 effects on the cell cycle are complex and neither is strictly required for cell cycle progression (Kozar et al., 2004; Sherr, 2000; Sherr and Roberts, 2004). They are non-catalytic activating subunits of cyclin-dependent kinases 4 and 6 (Cdk4/6) that promote the phosphorylation of Rb, which in turn removes Rb suppression to promote cell cycle progression and induce the E2F family of transcription factors (Ohnuma and Harris, 2003; Ross, 1996). Progenitor exit from the cell cycle requires reaching a threshold set by levels of cyclin D, opposed by levels of Cdk-inhibitors (CdkIs) including CIP/KIP-family CdkIs p21 (Cdkn1a), p27, p57 and INK-family members including p18 (Cdkn2c) and p19 (Cdkn2d). Among CdkIs, p27 inhibits cyclin E-Cdk2 action required for entry into S phase and p27 has a significant influence on brain size (Geng et al., 2001; Kiyokawa et al., 1996; Knoepfler et al., 2002). Inducible overexpression of p27 in embryonic mouse neural progenitors lengthens G1 specifically (Mitsuhashi et al., 2001). G1 cyclins D2 and D1 form complexes with CIP/KIP CdkIs including p27 and so oppose their cell cycle inhibitory action (Sherr, 2000). Indeed, genetic crosses between *cD1*- and *p27*-knockout mice demonstrate that reduced p27 compensates for lost cD1 (Geng et al., 2001). In addition, p27 has been implicated in the regulation of transit-amplifying divisions in adult neurogenesis (Doetsch et al., 2002), which are divisions most similar to those in the embryonic SVZ (Noctor et al., 2004). Phosphorylated Rb is also affected by cyclin loss and is another key component of terminal mitosis and differentiation of neurons (Ferguson and Slack, 2001; Ferguson et al., 2002). The present study demonstrates that the effects of cD1 and cD2 on the cell cycle within developing brain are not completely equivalent and their different roles in brain histogenesis may hinge on their distinct effects on p27 and pRb.

How might these cell cycle relationships be understood in the context of the embryonic proliferative ventricular epithelium (PVE)? Recent studies of embryonic PVE behavior indicate that the VZ and SVZ represent two distinct niches of progenitor divisions in which the SVZ supports proliferation of an intermediate progenitor similar to the transit-amplifying divisions of adult neurogenesis in the SVZ and hippocampus (Doetsch et al., 1999; Noctor et al., 2004; Seri et al., 2001). The present study supports a model in which cD2 is required to promote the intermediate progenitor divisions in the SVZ and that these transit-amplifying divisions are necessary to generate the normal complement of PV-expressing interneurons in cortex and hippocampus (Fig. 8B-D). In this model, cD2 suppresses p27 expression and promotes phosphorylation of Rb. In the WT MGE (Fig. 8B), cD2 is induced in cells entering the SVZ, where suppression of p27 and promotion of pRb favor intermediate progenitor proliferation and an appropriate balance of SSN+ and PV+ interneurons. When cD2 is absent (Fig. 8C), p27 is unopposed and reduced levels of pRb hinder transit-amplifying divisions, resulting in a reduced density of PV+ interneurons, but a normal density of SSN+ interneurons (although the absolute numbers of subtype cells are reduced). By contrast, loss of cD1 (Fig. 8D) induces cD2 in the $cD1^{-/-}$ VZ, which suppresses p27 expression and promotes pRb levels in the VZ, while cD2 in the SVZ continues to support intermediate progenitor divisions. Although these cD2-supported divisions may progress more slowly (Glickstein et al., 2007), the normal balance between progenitor and intermediate progenitor divisions is maintained, resulting in normal densities of SSN+ and PV+ interneurons in *cD1* nulls.

Further studies will determine how cD2 can suppress p27 – whether through transcriptional or post-transcriptional events. The data here do not address whether cD2 expression influences not only proliferation, but also the gene expression routines that specify interneuron subtypes (and that are only partially delineated). Nevertheless, the present studies illuminate differences in the impact of cD2 and cD1 on progenitor division and underscore the important contribution of cell cycle control to regional patterning in the developing brain.

This work was supported by NIH P01 NS048120 to M.E.R., H.M. and S.B.G.

Supplementary material

Supplementary material for this article is available at
http://dev.biologists.org/cgi/content/full/134/22/4083/DC1

References

Ango, F., di Cristo, G., Higashiyama, H., Bennett, V., Wu, P. and Huang, Z. J. (2004). Ankyrin-based subcellular gradient of neurofascin, an immunoglobulin family protein, directs GABAergic innervation at purkinje axon initial segment. *Cell* **119**, 257-272.

Bhide, P. G. (1996). Cell cycle kinetics in the embryonic mouse corpus striatum. *J. Comp. Neurol.* **374**, 506-522.

Butt, S. J., Fuccillo, M., Nery, S., Noctor, S., Kriegstein, A., Corbin, J. G. and Fishell, G. (2005). The temporal and spatial origins of cortical interneurons predict their physiological subtype. *Neuron* **48**, 591-604.

Ciemerych, M. A., Kenney, A. M., Sicinska, E., Kalaszczynska, I., Bronson, R. T., Rowitch, D. H., Gardner, H. and Sicinski, P. (2002). Development of mice expressing a single D-type cyclin. *Genes Dev.* **16**, 3277-3289.

Cobos, I., Calcagnotto, M. E., Vilaythong, A. J., Thwin, M. T., Noebels, J. L., Baraban, S. C. and Rubenstein, J. L. (2005). Mice lacking Dlx1 show subtype-specific loss of interneurons, reduced inhibition and epilepsy. *Nat. Neurosci.* **8**, 1059-1068.

Constantinidis, C. and Goldman-Rakic, P. S. (2002). Correlated discharges among putative pyramidal neurons and interneurons in the primate prefrontal cortex. *J. Neurophysiol.* **88**, 3487-3497.

Derchansky, M., Shahar, E., Wennberg, R. A., Samoilova, M., Jahromi, S. S., Abdelmalik, P. A., Zhang, L. and Carlen, P. L. (2004). Model of frequent, recurrent, and spontaneous seizures in the intact mouse hippocampus. *Hippocampus* **14**, 935-947.

Doetsch, F., Caille, I., Lim, D. A., Garcia-Verdugo, J. M. and Alvarez-Buylla, A. (1999). Subventricular zone astrocytes are neural stem cells in the adult mammalian brain. *Cell* **97**, 703-716.

Doetsch, F., Verdugo, J. M., Caille, I., Alvarez-Buylla, A., Chao, M. V. and Casaccia-Bonnefil, P. (2002). Lack of the cell-cycle inhibitor p27Kip1 results in selective increase of transit-amplifying cells for adult neurogenesis. *J. Neurosci.* **22**, 2255-2264.

Eagleson, K. L., Bonnin, A. and Levitt, P. (2005). Region- and age-specific deficits in gamma-aminobutyric acidergic neuron development in the telencephalon of the uPAR(–/–) mouse. *J. Comp. Neurol.* **489**, 449-466.

Ferguson, K. L. and Slack, R. S. (2001). The Rb pathway in neurogenesis. *NeuroReport* **12**, A55-A62.

Ferguson, K. L., Vanderluit, J. L., Hebert, J. M., McIntosh, W. C., Tibbo, E., MacLaurin, J. G., Park, D. S., Wallace, V. A., Vooijs, M., McConnell, S. K. et al. (2002). Telencephalon-specific Rb knockouts reveal enhanced neurogenesis, survival and abnormal cortical development. *EMBO J.* **21**, 3337-3346.

Freund, T. F. and Buzsaki, G. (1996). Interneurons of the hippocampus. *Hippocampus* **6**, 347-470.

Geng, Y., Yu, Q., Sicinska, E., Das, M., Bronson, R. T. and Sicinski, P. (2001). Deletion of the p27Kip1 gene restores normal development in cyclin D1-deficient mice. *Proc. Natl. Acad. Sci. USA* **98**, 194-199.

Glickstein, S. B., Alexander, S. and Ross, M. E. (2007). Differences in cyclin d2 and d1 protein expression distinguish forebrain progenitor subsets. *Cereb. Cortex* **17**, 632-642.

Hartman, K. N., Pal, S. K., Burrone, J. and Murthy, V. N. (2006). Activity-dependent regulation of inhibitory synaptic transmission in hippocampal neurons. *Nat. Neurosci.* **9**, 642-649.

Huard, J. M., Forster, C. C., Carter, M. L., Sicinski, P. and Ross, M. E. (1999). Cerebellar histogenesis is disturbed in mice lacking cyclin D2. *Development* **126**, 1927-1935.

Kawaguchi, Y. and Kubota, Y. (1998). Neurochemical features and synaptic connections of large physiologically-identified GABAergic cells in the rat frontal cortex. *Neuroscience* **85**, 677-701.

Kiyokawa, H., Kineman, R. D., Manova-Todorova, K. O., Soares, V. C., Hoffman, E. S., Ono, M., Khanam, D., Hayday, A. C., Frohman, L. A. and Koff, A. (1996). Enhanced growth of mice lacking the cyclin-dependent kinase inhibitor function of p27(Kip1). *Cell* **85**, 721-732.

Knoepfler, P. S., Cheng, P. F. and Eisenman, R. N. (2002). N-myc is essential during neurogenesis for the rapid expansion of progenitor cell populations and the inhibition of neuronal differentiation. *Genes Dev.* **16**, 2699-2712.
Kozar, K., Ciemerych, M. A., Rebel, V. I., Shigematsu, H., Zagozdzon, A., Sicinska, E., Geng, Y., Yu, Q., Bhattacharya, S., Bronson, R. T. et al. (2004). Mouse development and cell proliferation in the absence of D-cyclins. *Cell* **118**, 477-491.
Marin, O., Anderson, S. A. and Rubenstein, J. L. (2000). Origin and molecular specification of striatal interneurons. *J. Neurosci.* **20**, 6063-6076.
Mitsuhashi, T., Aoki, Y., Eksioglu, Y. Z., Takahashi, T., Bhide, P. G., Reeves, S. A. and Caviness, V. S., Jr (2001). Overexpression of p27Kip1 lengthens the G1 phase in a mouse model that targets inducible gene expression to central nervous system progenitor cells. *Proc. Natl. Acad. Sci. USA* **98**, 6435-6440.
Noctor, S. C., Martinez-Cerdeno, V., Ivic, L. and Kriegstein, A. R. (2004). Cortical neurons arise in symmetric and asymmetric division zones and migrate through specific phases. *Nat. Neurosci.* **7**, 136-144.
Ohnuma, S. and Harris, W. A. (2003). Neurogenesis and the cell cycle. *Neuron* **40**, 199-208.
Paxinos, G. and Franklin, K. B. J. (2001). *The Mouse Brain in Stereotaxic Coordinates*. San Diego: Academic Press.
Peters, A., Palay, S. L. and Webster, H. d. F. (1991). *The Fine Structure of the Nervous System: Neurons and their Supporting Cells*. New York: Oxford University Press.
Powell, E. M., Campbell, D. B., Stanwood, G. D., Davis, C., Noebels, J. L. and Levitt, P. (2003). Genetic disruption of cortical interneuron development causes region- and GABA cell type-specific deficits, epilepsy, and behavioral dysfunction. *J. Neurosci.* **23**, 622-631.
Ross, M. E. (1996). Cell division and the nervous system: regulating the cycle from neural differentiation to death. *Trends Neurosci.* **19**, 62-68.
Roy, K., Thiels, E. and Monaghan, A. P. (2002). Loss of the tailless gene affects forebrain development and emotional behavior. *Physiol. Behav.* **77**, 595-600.
Schmitz, C. and Hof, P. R. (2000). Recommendations for straightforward and rigorous methods of counting neurons based on a computer simulation approach. *J. Chem. Neuroanat.* **20**, 93-114.
Seri, B., Garcia-Verdugo, J. M., McEwen, B. S. and Alvarez-Buylla, A. (2001). Astrocytes give rise to new neurons in the adult mammalian hippocampus. *J. Neurosci.* **21**, 7153-7160.
Sherr, C. J. (2000). The Pezcoller lecture: cancer cell cycles revisited. *Cancer Res.* **60**, 3689-3695.
Sherr, C. J. and Roberts, J. M. (2004). Living with or without cyclins and cyclin-dependent kinases. *Genes Dev.* **18**, 2699-26711.
Sicinski, P., Donaher, J. L., Parker, S. B., Li, T., Fazeli, A., Gardner, H., Haslam, S. Z., Bronson, R. T., Elledge, S. J. and Weinberg, R. A. (1995). Cyclin D1 provides a link between development and oncogenesis in the retina and breast. *Cell* **82**, 621-630.
Sicinski, P., Donaher, J. L., Geng, Y., Parker, S. B., Gardner, H., Park, M. Y., Robker, R. L., Richards, J. S., McGinnis, L. K., Biggers, J. D. et al. (1996). Cyclin D2 is an FSH-responsive gene involved in gonadal cell proliferation and oncogenesis. *Nature* **384**, 470-474.
Stork, O., Ji, F. Y., Kaneko, K., Stork, S., Yoshinobu, Y., Moriya, T., Shibata, S. and Obata, K. (2000). Postnatal development of a GABA deficit and disturbance of neural functions in mice lacking GAD65. *Brain Res.* **865**, 45-58.
Swanwick, C. C., Murthy, N. R., Mtchedlishvili, Z., Sieghart, W. and Kapur, J. (2006). Development of gamma-aminobutyric acidergic synapses in cultured hippocampal neurons. *J. Comp. Neurol.* **495**, 497-510.
Vaughan, D. W. (1984). The structure of neuroglial cells. In *Functional Properties of Cortical Cells*. Vol. 2 (ed. E. G. Jones and A. Peters), pp. 285-239. New York: Plenum.
Wang, Y., Gupta, A., Toledo-Rodriguez, M., Wu, C. Z. and Markram, H. (2002). Anatomical, physiological, molecular and circuit properties of nest basket cells in the developing somatosensory cortex. *Cereb. Cortex* **12**, 395-410.
West, M. J., Slomianka, L. and Gundersen, H. J. (1991). Unbiased stereological estimation of the total number of neurons in the subdivisions of the rat hippocampus using the optical fractionator. *Anat. Rec.* **231**, 482-497.
Wonders, C. P. and Anderson, S. A. (2006). The origin and specification of cortical interneurons. *Nat. Rev. Neurosci.* **7**, 687-696.
Xu, Q., de la Cruz, E. and Anderson, S. A. (2003). Cortical interneuron fate determination: diverse sources for distinct subtypes? *Cereb. Cortex* **13**, 670-676.
Xu, Q., Cobos, I., De La Cruz, E., Rubenstein, J. L. and Anderson, S. A. (2004). Origins of cortical interneuron subtypes. *J. Neurosci.* **24**, 2612-2622.